1-1-2021

Cross-Mixing Hybrid Beamformer for Wideband Apertures

Rimon Hokayem
Florida International University

Sandhiya Reddy Govindarajulu
Florida International University

Elias A. Alwan
Florida International University

John L. Volakis
Florida International University

IEEE Access
Multidisciplinary | Rapid Review | Open Access Journal

Received March 16, 2021, accepted April 13, 2021, date of publication April 16, 2021, date of current version April 26, 2021.

Digital Object Identifier 10.1109/ACCESS.2021.3073866

Cross-Mixing Hybrid Beamformer for Wideband Apertures

RIMON HOKAYEM, (Graduate Student Member, IEEE), SANDHIYA REDDY GOVINDARAJULU, (Graduate Student Member, IEEE), ELIAS A. ALWAN, (Member, IEEE), AND JOHN L. VOLAKIS, (Fellow, IEEE)
Department of Electrical and Computer Engineering, Florida International University, Miami, FL 33174, USA
Corresponding author: Rimon Hokayem (rhoka001@fiu.edu)

This work was funded by the National Science Foundation under the grant awards 1731649 and 1943040.

ABSTRACT Existing beamforming arrays suffer from the size and cost of the RF front-end and digital back-end components. In this paper, a novel hybrid beamforming configuration for wideband receivers is introduced. The design replaces phase shifters and local oscillators (LO) with cross mixing antenna elements to maximize diversity gain. In this paper, an analytical model of the cross mixing beamformer (CMB) is first presented. Simulations are carried out showing that a maximum diversity gain can be achieved with the CMB approach. Two prototypes were implemented using 2×1 and 4×2 element arrays and tested at 2.31 GHz. Measured results show that CMB achieves coherent signal combining and can preserve the phase delay information needed for hybrid beamforming setups.

INDEX TERMS Antenna arrays, antenna subarrays, beamforming, frontend circuitry, front end circuits and systems, RF front ends, self-mixing, self-mixing array, self-mixing subarray, wideband apertures, wide beamwidth.

I. INTRODUCTION

Future 5G communications links are expected to support data rates 50 times faster than the current 4G Long-Term Evolution (LTE) networks. The enabling infrastructure is radio frequency (RF) front-ends capable of handling this data increase using wideband, but also very small in size, weight, and low power. As such, there is a growing interest for reduced size ultra-wideband (UWB) apertures and RF electronics to enable compact integration on small platforms. Concurrently, the small size of RF devices and antenna apertures for the emerging 5G bands provides an impetus for realizing low profile and portable systems.

To compensate for the higher losses associated with the 5G bands [1], high gain beamforming systems are required. However, traditional analog [2]–[6] and digital [7]–[10] beamformers suffer from intensive hardware requirements. More in details, analog beamformers employ phase shifters at the RF front-end [2]–[4] or at the local oscillator (LO) [5], [6], as depicted in Fig. 1a and 1b, respectively. In both cases, hardware modification or a phase control biasing system is required to account for all possible angles of arrival (AoA). As such, analog beamformers have limited spatial diversity. In contrast, digital beamformers perform amplitude scaling and shifting operations in the digital domain, as depicted in Fig. 1c [7]–[10]. As opposed to analog beamforming approaches, digital beamformers offer flexibility and multi-beam generation [11]. However, digital configurations require an analog-to-digital converter (ADC) for each antenna element, implying high cost, size, and power consumption.

To reduce hardware requirements, hybrid beamformers [12]–[15] present an improved solution by combining both analog and digital techniques, as depicted in Fig. 1e. The antenna array is first divided into multiple sub-arrays. Then, analog beamforming is performed in each sub-array using phase shifters. This technique leads to a reduction in the number of ADCs to only 1 per sub-array. However, hybrid beamfomers remain restricted by the spatial resolution and frequency of operation imposed by the phase shifters.

Recent topologies have employed the self-mixing concept [16] instead of phase shifters to eliminate phase delays associated with a specific AoA. In other words, mixing antenna element signals with themselves can potentially allow for coherent signal combining and maximum diversity gain. Notably, recently proposed self-mixing

The associate editor coordinating the review of this manuscript and approving it for publication was Engang Tian.

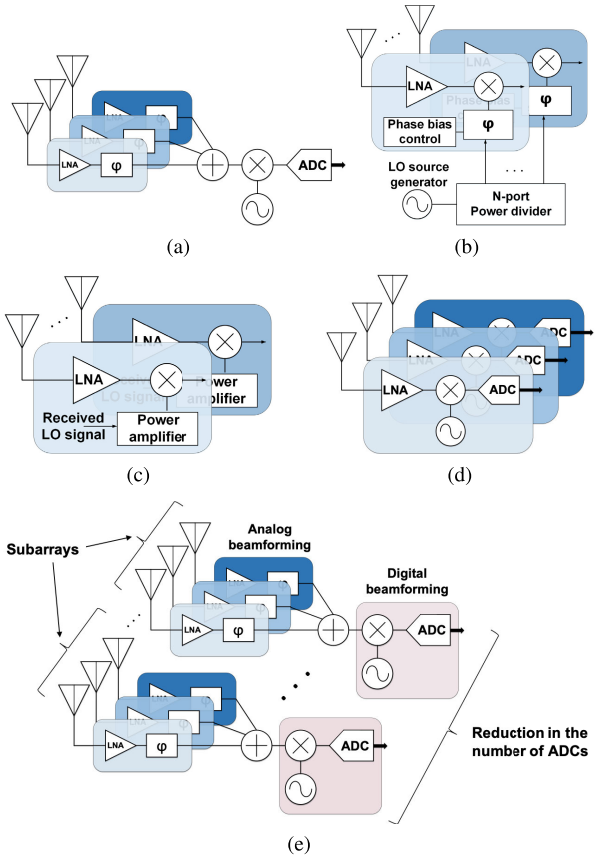

FIGURE 1. Schematic of (a) RF-phase shifting beamforming, (b) LO-phase shifting beamforming, (c) self-mixing beamforming, (d) digital beamforming, and (e) hybrid beamforming architectures.

beamformers [16] can offer broad receive patterns with a much finer resolution as compared to traditional beamformers. However, the wide spatial coverage makes self-mixing techniques more vulnerable to interference from other users in a multi-user environment. We note that, signals at all antenna elements become in phase after self-mixing. As such, this approach is limited to analog beamforming topologies. Conversely, cross-mixing elements preserves the phase delays between sub-arrays, and hence can be used with hybrid beamforming configurations [17].

In this paper, we present a novel RF **C**ross-**M**ixing hybrid **B**eamforming (CMB) technique for sub-6GHz 5G bands, as depicted in Fig. 2, based on an element-to-element mixing to achieve phase coherence in a sub-array. Our architecture avoids the use of 1) analog phase shifters and bias control circuitry and 2) LO sources, implying single chip integration. Importantly, cross-mixing avoids the limitations and requirements of phase tuning, such as 1) fast response to control signals, 2) amplitude changes as phase state changes, 3) isolation between the phase control switches, 4) phase error and resolution limitation, 5) flat phase response over the frequency band of interest. Therefore, our design provides much finer angular resolution and phase delay cancellation without the need for external bias control signals.

The paper is structured as follows: Section II provides an overview of the self-mixing technique and its adaptation to antenna array design. Section III gives a description of the CMB architecture in linear array configurations. Section IV gives the array factor of the cross-mixing design and decribes the CMB in a sub-array setting. Sections V extends the analysis to planar array and sub-array settings. Section VI provides simulations and measurements to validate the CMB concept in sub-array configurations.

II. SELF-MIXING TECHNIQUES

Self-mixing receivers often use a simple diode mixer [18] to beat the received signals with one another. This approach removes the need for phase shifters, simplifying the receiver's front-end, and the LO source is eliminated. This reduces significantly the size and cost of the receiver. [18] removes the need for a physical LO source. However, self-mixing has the drawback of SNR degradation [19], [20]. Also, there is a challenge with power balancing as the transmitted carrier and information signals must be of equal power to achieve the best conversion performance [19]. This implies that half of the used power holds no information. For this reason, other designs [21] use a low power carrier signal that is separately amplified at the receiver via a power amplifier. Alternatively, a frequency locking scheme [22]–[24] can be employed at the receiver to lock its frequency to the carrier. As such, the oscillator provides a fixed LO power for the

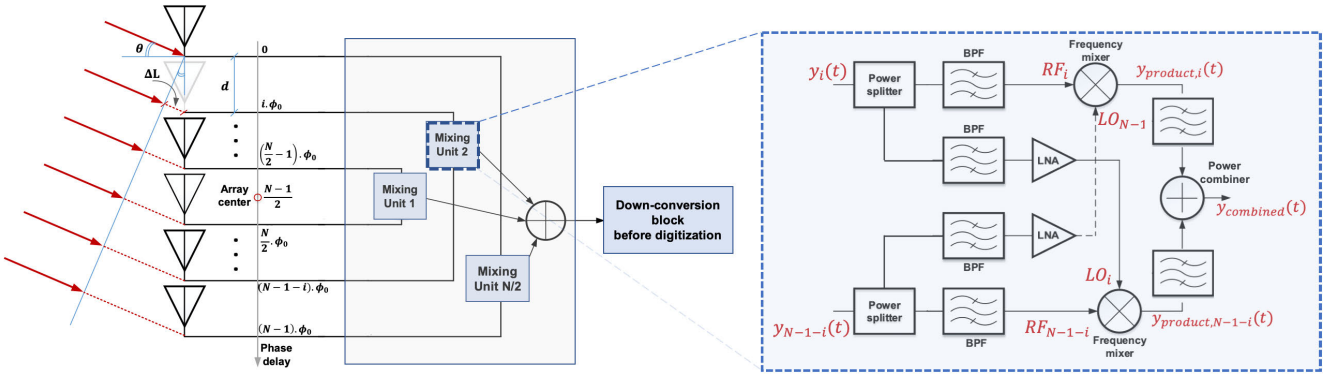

FIGURE 2. Cross-mixing beamforming (CMB) for a pair of elements from opposite sides of the array center.

mixing process regardless of the received signal power level. However, [22]–[24] are restricted to the range of the received LO power needed for achieving locking state.

Other designs [25] employ phase-locked loops (PLLs). For this approach, the carrier signal is used to lock the PLL to generate a stable LO signal. However, such receivers suffer from the added size, cost, and power consumption due to the needed LO synthesizers. Receiver complexity also varies with signal modulation and symbol rates, implying calibration. As such, receivers with PLL schemes exacerbates efficiency and complexity when employed with large antenna arrays.

Based on the above, simple, stable, low power, and low complexity self-mixing designs are needed for large arrays. For instance, an example of a simple design employs diodes for self-mixing [16]. However, as mentioned earlier, all self-mixing techniques are incompatible with hybrid beamformers.

In this paper, a novel CMB architecture is presented for hybrid beamformer techniques. As opposed to self-mixing designs, in CMB, we mix signals from antenna pairs that are symmetrically located with respect to the center of the array. This CMB approach is depicted in Fig. 2. Compared to [17], [26], each element cross-mixes with the opposite element via a separate mixer to avoid information loss. Also, our proposed design removes phase-locked loops [27] to significantly reduce hardware requirements and improve stability. Notably, similarly to [21], the new design employs low noise amplifiers (LNAs) to amplify the signals from the oppositely placed antenna elements to achieve the best conversion performance.

Using the presented CMB, a sub-array beamforming can be realized, as depicted in Fig. 3. That is, cross-mixing can be further integrated with digital beamforming, not feasible with other designs [16]. Further filtering in the digital back-end controls the beam pattern to the desired direction.

As with all conventional receivers, gain and phase mismatches between the antenna elements and RF chains limit the precision of self-mixing beamformers that can be achieved in practice. The resulting errors can be compensated for by a one-time calibration for fixed errors resulting from fabrication tolerance and imbalance between antenna and RF elements, or by real-time periodic re-calibration to account for random channel variations such as changes in receiver noise temperature and voltage drifts. That is, delay lines or phase shifters with phase control units can be used to account for the phase mismatches.

III. CROSS-MIXING BEAMFORMER ARCHITECTURE

To demonstrate the operation of the CMB architecture, a signal model is first derived and subsequently validated via simulations. To start with, we assume a transmitted signal, expressed as:

$$s(t) = A_{RF}cos(2\pi f_{RF}t + \phi_{RF}) + A_{LO}cos(2\pi f_{LO}t + \phi_{LO}) \quad (1)$$

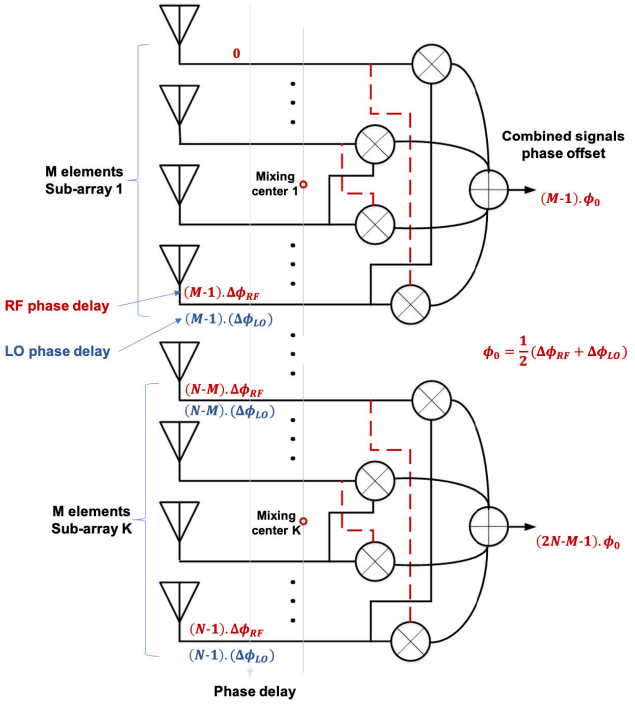

FIGURE 3. Sub-arraying with CMB showing that the output of each sub-array retains the phase delay information required for digital beamforming operations.

where A_{RF} and A_{LO} denote the amplitude coefficients of the RF and the LO signals, respectively. The frequencies f_{RF} and f_{LO} refer to the RF and LO frequencies, whereas ϕ_{RF} and ϕ_{LO} represent the corresponding signal phases. We remark that channel noise is omitted in this study, as our concern is to only study signal phase delays. Also, the RF signal in (1) can be assumed to be narrowband with a fractional bandwidth $\leq 1\%$.

At the receiver's side, we assume a uniform linearly spaced antenna array having an even number of antenna elements N, as illustrated in Fig. 2. A signal arriving at an angle θ away from broadside implies a progressive time delay, ΔT, given by

$$\Delta T = \frac{\Delta L}{c} = \frac{dsin\theta}{c} \quad (2)$$

In the above, ΔL is the distance travelled by the wave to reach the adjacent antenna element, c speed of light, and d is the distance between adjacent array elements. The received signal at the i^{th} antenna element can then be expressed as:

$$y_i(t) = y(t + i\Delta T) = A_{RF}cos\left[2\pi f_{RF}(t + i\Delta T) + \phi_{RF}\right] + A_{LO}cos\left[2\pi f_{LO}(t + i\Delta T) + \phi_{LO}\right] \quad (3)$$

Using (2), the corresponding phase delay $\Delta\phi_{RF}$ of the received RF signal is given by

$$\Delta\phi_{RF} = 2\pi f_{RF}\Delta T = \frac{2\pi f_{RF}dsin\theta}{c} = \frac{2\pi dsin\theta}{\lambda_{RF}} \quad (4)$$

Similarly, the phase delay of the received LO signal is given by

$$\Delta\phi_{LO} = 2\pi f_{LO}\Delta T = \frac{2\pi d sin\theta}{\lambda_{LO}} \tag{5}$$

Using the above, (3) gives

$$y_i(t) = A_{RF}cos(2\pi f_{RF}t + i\Delta\phi_{RF}) + A_{LO}cos(2\pi f_{LO}t + i\Delta\phi_{LO}) \tag{6}$$

where we set $\phi_{RF} = \phi_{LO} = 0$ since only $\Delta\phi_{RF}$ and $\Delta\phi_{LO}$ are relevant to the subsequent analysis.

As shown in Fig. 2, $y_i(t)$ is passed through a power divider. Bandpass filters are then used to filter out the desired LO and RF signals. The LO signal is subsequently amplified, LO_i, and fed to the opposite element chain for mixing with its corresponding filtered RF signal, RF_{N-1-i}. We note that, as with conventional self-mixing receivers, the received LO signal power is usually equal or less than the RF signal, and hence cannot drive the mixer. Therefore, after filtering, a proper amplification is crucial to ensure that the LO signal is at least 10-15dB higher than the RF signal at the mixer port.

Next, following the circuit in Fig. 2, the RF signal from the i^{th} antenna element, RF_i, is mixed with the signal from the $(N-1-i)^{th}$ element, LO_{N-1-i}, to generate $y_{product,i}(t)$ for the i^{th} front-end chain. Similarly, the signal from the i^{th} antenna element, LO_i, is mixed with the RF signal from the $(N-1-i)^{th}$ element, RF_{N-1-i}, to generate $y_{product,N-1-i}(t)$ for the $(N-1-i)^{th}$ chain. That is, pairs from opposite sides of the array center are mixed. Notably, for an array of N antenna elements, this CMB architecture yields N mixing processes.

Setting $A_{LO} = A_{RF} = 1$ and assuming no conversion losses, the resulting output after mixing RF_i and the LO signal from the symmetrically opposite side of the array, *viz.* the LO_{N-1-i} signal, gives

$$y_{product,i}(t) = cos(2\pi f_{RF}t + i\Delta\phi_{RF}) \times cos\left[2\pi f_{LO}t + (N-1-i)\Delta\phi_{LO}\right] \tag{7}$$

As such, after filtering we get (see Fig. 2)

$$y_{product,i}(t) = cos\left[2\pi f_{RF+LO}t + i\Delta\phi_{RF} + (N-1-i)\Delta\phi_{LO}\right] \tag{8}$$

$$\begin{aligned} y_{product,N-1-i}(t) &= cos\left[2\pi f_{RF}t + (N-1-i)\Delta\phi_{RF}\right] \\ &\quad \times cos(2\pi f_{LO}t + i\Delta\phi_{LO}) \\ &= cos\left[2\pi f_{RF+LO}t + (N-1-i)\Delta\phi_{RF} + i\Delta\phi_{LO}\right] \end{aligned} \tag{9}$$

Doing so for all array element pairs, we have

$$\begin{aligned} y_{combined}(t) &= 2\sum_{i=0}^{\frac{N}{2}-1} cos\left[\frac{N-1-2i}{2}(\Delta\phi_{RF} - \Delta\phi_{LO})\right] \\ &\quad \times cos\left[2\pi f_{RF+LO}t + \frac{N-1}{2}(\Delta\phi_{RF} + \Delta\phi_{LO})\right] \end{aligned} \tag{10}$$

From (10), it is apparent that to achieve coherent combining, we need

$$cos\left[\frac{N-1-2i}{2}(\Delta\phi_{RF} - \Delta\phi_{LO})\right] \approx 1 \tag{11}$$

This implies that the LO frequency must equal the RF frequency. The latter is interpreted as setting $\Delta\phi_{LO} = \Delta\phi_{RF}$, *viz.* $f_{LO} = f_{RF}$.

But concurrently, it is important to keep the RF and LO frequencies different to achieve low noise reception. Accordingly, a compromise in the choice of f_{RF} and f_{LO} is needed.

In a effort for a compromise, the condition (11) can be modified to read

$$cos\left[\frac{N-1-2i}{2}(\Delta\phi_{RF} - \Delta\phi_{LO})\right] \geq 0.9 \approx cos(\frac{5\pi}{36}) \tag{12}$$

This condition is equivalent to achieving a theoretical array gain up to 90% of its maximum value. Using (12), the corresponding condition on the LO frequency is

$$f_{RF} - \frac{5c}{36(N-1)d} \leq f_{LO} \leq f_{RF} + \frac{5c}{36(N-1)d} \tag{13}$$

We will employ this condition in our subsequent analysis.

IV. CMB ARRAY FACTOR

Using the CMB concept in Fig. 2, the corresponding array factor is

$$AF = \left[e^{j(N-1)k'dcos\theta} + e^{jkdcos\theta} \times e^{j(N-2)k'dcos\theta} + \ldots + e^{j(N-1)kdcos\theta}\right] \tag{14}$$

where $k' = \frac{2\pi}{\lambda_{LO}}$.

Using (14), the total array pattern E_t can be expressed as

$$E_t(\theta) = E_e(\theta) \times AF \tag{15}$$

where $E_e(\theta)$ is the element pattern.

When $f_{LO} = f_{RF}$, (14) becomes

$$AF = N\left[e^{j(N-1)kdcos\theta}\right] \tag{16}$$

As expected, the magnitude of the array factor is equal to N. In other words, CMB achieves maximum array factor gain that is independent of the angle of arrival. In this case, the total array pattern E_t only varies with the element pattern.

In the case of hybrid beamformers, a large array is first divided into multiple sub-arrays. Each sub-array can employ the CMB concept as in Fig. 3, using (10) and (13). Specifically, in (10), we showed that the resulting phase of the combined signal is equivalent to the summation of the first and last elements of the array, *viz.* $(N-1)\phi_0$, where

$$\phi_0 = \frac{1}{2}\left[\Delta\phi_{RF} + \Delta\phi_{LO}\right] \tag{17}$$

Accordingly, as depicted in Fig. 3, the first sub-array combines signals with an offset of $(M-1)\phi_0$, the second sub-array yields an offset of $(3M-1)\phi_0$, and so on. This implies a phase difference between adjacent sub-arrays of $2M\phi_0$

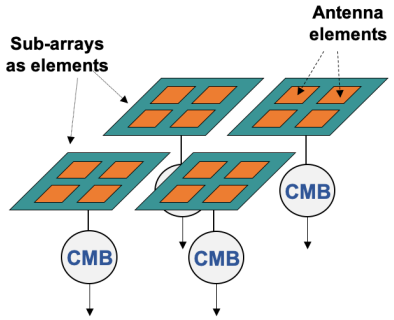

FIGURE 4. A full-array of sub-arrays as individual elements.

(for sub-arrays with M elements). As such, cross-mixing can be used with subsequent digital beamforming designs.

With a sub-array configuration, the total array pattern is

$$E_t(\theta) = E_e(\theta) \times AF_t(\theta) \tag{18}$$

with AF_t described as

$$AF_t(\theta) = AF_{sub}(\theta) \times AF_{full}(\theta) \tag{19}$$

where AF_{sub} is the array factor of one sub-array as described in (14). AF_{full} is the full array factor considering sub-arrays as individual elements [28], as shown in Fig. 4. Using (17), AF_{full} can be expressed as follows

$$AF_{full}(\theta) = \left[1 + e^{j\{2M\phi_0\}} + \ldots + e^{j\{2M(\frac{N}{M}-1)\phi_0\}}\right] \tag{20}$$

V. TWO-DIMENSIONAL CROSS-MIXING ARRAY

In this Section, a signal model is derived considering a two-dimensional array. To achieve the symmetry required for CMB, the antenna pairs are mixed according to the numbering scheme shown in Fig. 5. We assume that the reference antenna element is located at $(x = 0, y = 0)$. Thus, the coordinates of each antenna element are given by

$$d_{xy} = (xd_x,\ yd_y) \tag{21}$$

where d_x and d_y are the distances between the adjacent antenna elements in the x and y axes, respectively, such as $(d_x, d_y) \leq \lambda_{RF}/2$.

For an angle of arrival defined by the elevation and azimuth angles ψ and θ, respectively, the phase delay at each antenna element can be expressed as

$$\Delta\phi_{(x,y)} = \frac{2\pi}{\lambda} \sin\psi(xd_x \cos\theta + yd_y \sin\theta) \tag{22}$$

That is, the received signal can be written as

$$s_{xy}(t) = cos(2\pi f_{RF}t + \Delta\phi_{(x,y),RF}) + cos(2\pi f_{LO}t + \Delta\phi_{(x,y),LO}) \tag{23}$$

where $\Delta\phi_{(x,y),RF}$ and $\Delta\phi_{(x,y),LO}$ represent the signal phases of f_{RF} and f_{LO}, respectively.

Thus, by combining every cross-mixed pair of elements together, the resulting signal can be expressed as

$$s_{combined}(t) = A_{combined} \times \cos\{2\pi f_{RF+LO}t + \Delta\phi_{combined}\} \tag{24}$$

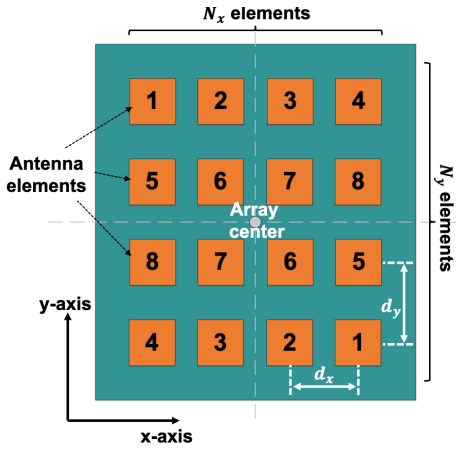

FIGURE 5. CMB mixes every pair of antenna elements in symmetry about the array center and achieves coherent combining.

where

$$\Delta\phi_{combined} = \pi \sin\psi\{(N_x - 1)d_x \cos\theta + (N_y - 1)d_y \sin\theta\}\left[\frac{1}{\lambda_{RF}} + \frac{1}{\lambda_{LO}}\right] \tag{25}$$

where N_x and N_y are the total number of antenna elements in the x and y axes, respectively, and

$$A_{combined} = 2 \times \cos\left[\pi \sin\psi\{(N_x - 1 - 2x)d_x \cos\theta + (N_y - 1 - 2y)d_y \sin\theta\}(\frac{1}{\lambda_{RF}} - \frac{1}{\lambda_{LO}})\right] \tag{26}$$

As in the 1D case (refer to (12)), to achieve $\geq$ 90% of the maximum theoretical combining gain, the following condition must be met:

$$f_{RF} - \Delta_f \leq f_{LO} \leq f_{RF} + \Delta_f \tag{27}$$

where

$$\Delta_f = \frac{5c}{36|(N_x - 1)d_x \cos\theta_b + (N_y - 1)d_y \sin\theta_b|} \tag{28}$$

and θ_b satisfies the following

$$(N_x - 1)d_x \sin\theta_b = (N_y - 1)d_y \cos\theta_b \tag{29}$$

By setting $N_y = 0$ and $d_y = 0$ in (28) and (29), we validate (13) for linear arrays

$$\Delta_f = \frac{5c}{36(N_x - 1)d_x} \tag{30}$$

Further, as depicted in Fig. 6, cross-mixing in sub-array settings yields a phase delay between adjacent sub-arrays along the x and y axes of $2N_x\phi_{x_0}$ and $2N_y\phi_{y_0}$, respectively, where $\phi_{x_0} = \pi d_x \sin\psi \cos\theta\left[\frac{1}{\lambda_{RF}} + \frac{1}{\lambda_{LO}}\right]$ and $\phi_{y_0} = \pi d_y \sin\psi \sin\theta\left[\frac{1}{\lambda_{RF}} + \frac{1}{\lambda_{LO}}\right]$.

Finally, the 2D array pattern can also be expressed as (18) and (19), where

$$AF_{sub} \approx N_xN_y\left[e^{j\{(N_x-1)kd_x sin\psi cos\theta + (N_y-1)kd_y sin\psi sin\theta\}}\right] \tag{31}$$

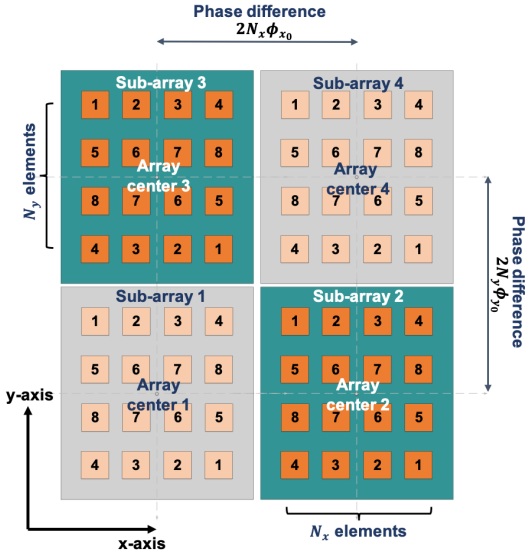

FIGURE 6. CMB in two-dimensional sub-array settings preserves the delay information between adjacent sub-arrays.

and

$$AF_{full}(\theta) = AF_{full,x}(\theta) \times AF_{full,y}(\theta) \tag{32}$$

$$AF_{full,x}(\theta) = \left[1 + e^{j\{2N_x\phi_{x_0}\}} + \ldots + e^{j\{2N_x(n_x-1)\phi_{x_0}\}}\right] \tag{33}$$

$$AF_{full,y}(\theta) = \left[1 + e^{j\{2N_y\phi_{y_0}\}} + \ldots + e^{j\{2N_y(n_y-1)\phi_{y_0}\}}\right] \tag{34}$$

where n_x and n_y are the number of sub-arrays along the x and y axes, respectively.

VI. SIMULATION AND EXPERIMENTAL VALIDATION

A. CMB IN LINEAR ARRAY CONFIGURATION

Simulations were conducted to validate the CMB concept. To do so, we considered an initial two-element array having an inter-element distance of $d = \lambda_{RF}/2$. Also, the RF frequency was set to $f_{RF} = 2.31\,GHz$, and using $1.67\ GHz \leq f_{LO} \leq 2.95\ GHz$. we chose $f_{LO} = 1.89\ GHz$. As depicted in the AWR analysis of Fig. 7, the RF and LO signals are received with additive white Gaussian noise (AWGN). Also, the incoming signal was incoming from $\theta = 90°$.

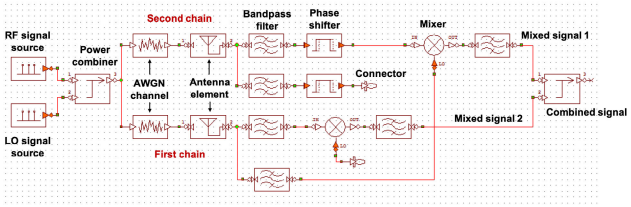

FIGURE 7. AWR simulation diagram of a two-element CMB concept.

Using (4) and (5), the equivalent phase delays of the RF and LO tones with $\theta = 90°$ will be $\Delta\phi_{RF} = 180°$ and $\Delta\phi_{LO} = 147°$, respectively. And as described in Fig. 2, the RF signal from one antenna is mixed with the LO signal of the second antenna. The resulting products imply a combined

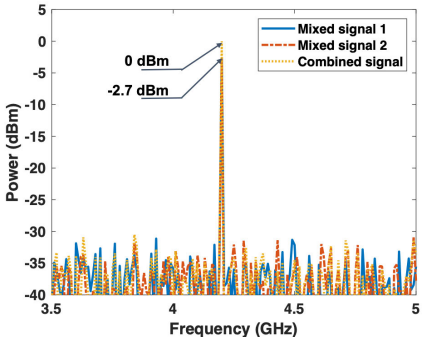

FIGURE 8. Simulations showing a 2.7 dB gain using CMB for a two-element array at AoA = 90°.

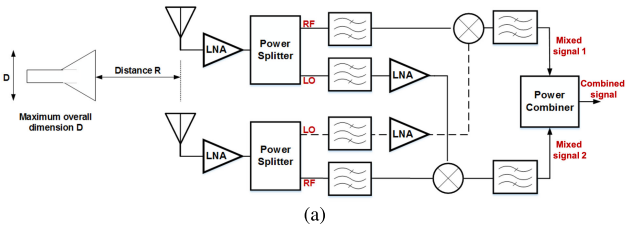

(a)

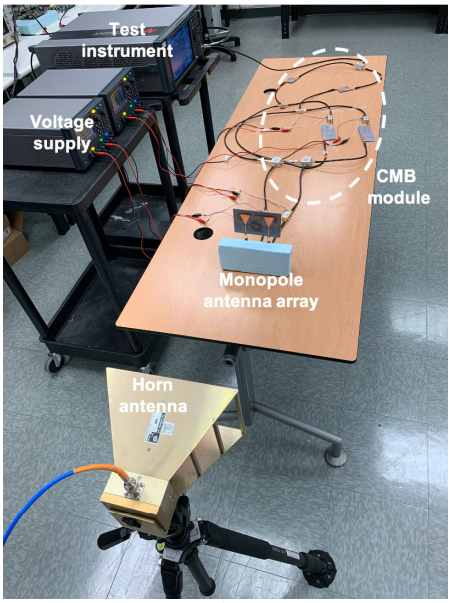

(b)

FIGURE 9. (a) Fabricated CMB for a two-element triangular monopole array. Testing was done indoors using a horn antenna for illumination, and (b) Experimental setup.

signal received at $f_{LO} + f_{RF} = 4.2$ GHz with a 3 dB gain. This is depicted in Fig. 8 showing that the CMB array gain is near its theoretical value.

A two-channel CMB was also fabricated and tested to demonstrate a proof-of-concept. This is depicted in Fig. 9 using commercial off-the-shelf (COTS) components. As above, we chose the RF and LO frequencies to be 2.31 GHz and 1.89 GHz, respectively. A two-element triangular monopole array receiver was fabricated, see Fig. 10, on a Rogers DiClad 880 substrate, having a dielectric constant

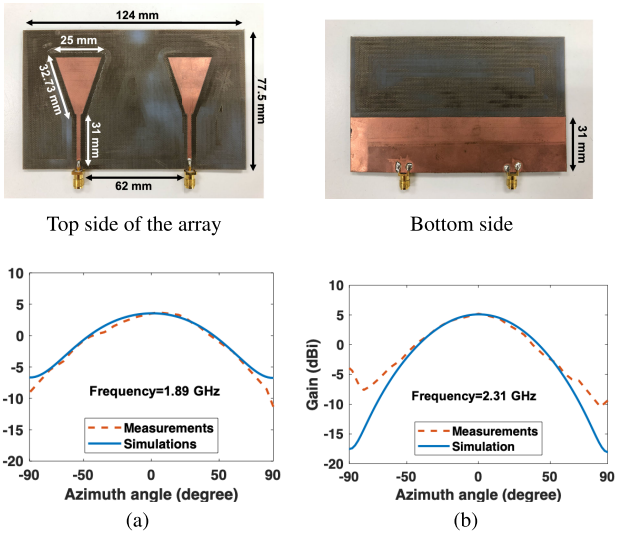

FIGURE 10. Radiation pattern of the two-element triangular CMB monopole array at (a) 1.89 GHz and (b) 2.31 GHz.

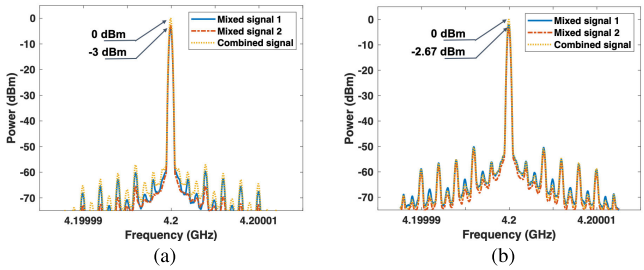

FIGURE 11. Normalized power plots showing the measured signal gain after cross-mixing two array element signals at symmetrically opposite locations within an array with incoming signal from a) $\theta = 0°$, (b) $\theta = 90°$.

of $\epsilon_r = 2.2$, a dielectric loss tangent $\tan\delta = 0.04$, and a thickness of 1.52 mm.

A link budget was also conducted to assess signal gain and losses at the RF and LO frequencies. To do so, we employed Friis link formula to express the received power, P_{RX} (dBm), as

$$P_{RX} = P_{TX} + G_{TX} + G_{RX} - L_{FS} - L_M \tag{35}$$

In the above, P_{TX} is the transmitted power (dBm), whereas G_{TX} and G_{RX} are the transmitter and receiver antenna gain (dBi), respectively. Further, L_M accounts for receiver circuit losses (dB), and L_{FS} is the free space path loss (dB) given by

$$L_{FS} = 20log_{10}(4\pi \frac{R}{\lambda}) \tag{36}$$

where R is the distance between the transmitter and receiver.

For our setup, we set[1] $R = 2m$ (*viz.* greater than $R_{far\ field}$). As such, (36) yields $L_{FS} = 45dB$ at the LO and RF frequencies, respectively. Notably, a 10 *dBi* horn antenna was used to transmit the $P_{TX} = 21$ *dBm* signals, as shown in Table 1.

[1]In our setup, $D = 0.3m$, and $\lambda_{max} = \lambda_{LO} = 0.158m$. As such, $R_{far\ field} \geq 1.134m$.

TABLE 1. Link budget estimation at 1.89 GHz and 2.31 GHz.

Frequency	LO at 1.89 GHz	RF at 2.31 GHz
Wavelength of the signals	0.158 m	0.129 m
Transmitted power	21 dBm	21 dBm
Transmit antenna gain	10 dBi	10 dBi
Receive antenna gain	3.5 dBi	5 dBi
Free space path loss	44 dB	45.7 dB
Miscellaneous losses	10 dB	10 dB
Received power	-19.5 dBm	-19.7 dB

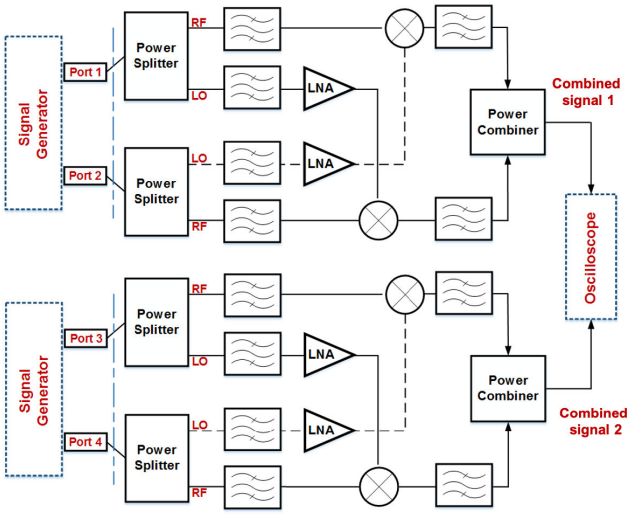

FIGURE 12. Schematic of the tested CMB design to study progressive phase between adjacent sub-arrays.

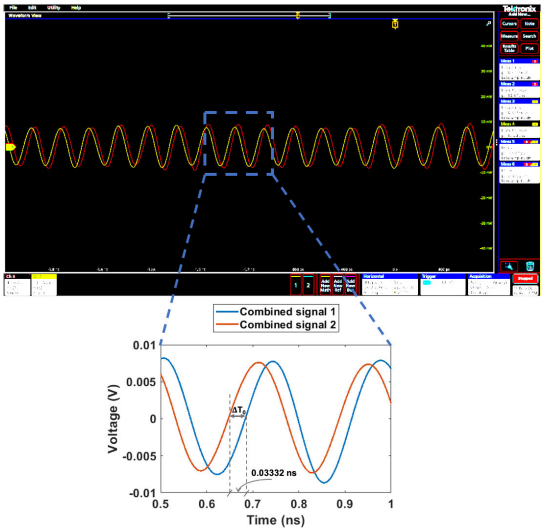

FIGURE 13. Oscilloscope screenshot showing that phase delay information is preserved after cross-mixing the sub-arrays at $\theta = 40°$.

Accordingly, (35) gives a received power of ~ -20 *dBm* at the RF and LO frequencies.

LNAs with 13 dB gain were used to amplify the received signals before feeding them to the CMB module, as shown in Fig. 9. Notably, the COTS mixers used in the test setup require a $\sim$7 *dBm* LO drive level. As such, the 13 dB LNAs were employed to also amplify the LO signal to $\sim$7 *dBm*.

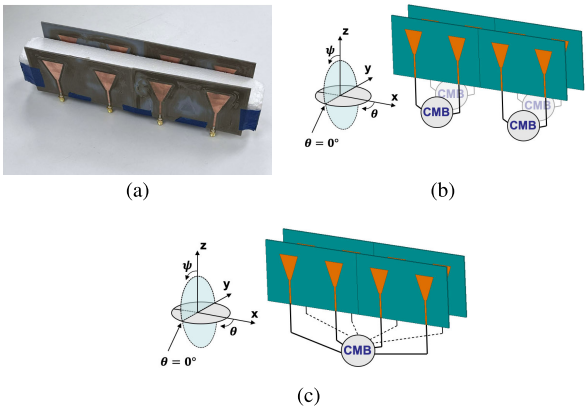

FIGURE 14. (a) Fabricated 4 × 2 monopole array. (b) Monopole array in sub-array setting. (c) Monopole array with 8-element CMB module.

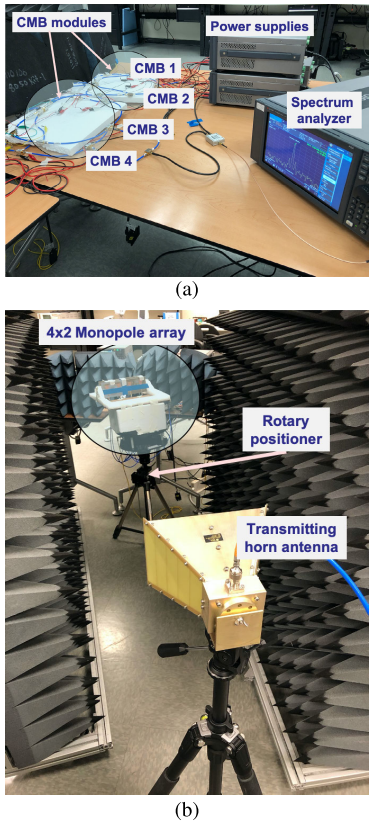

FIGURE 15. Experimental setup of a 4 × 2 triangular monopole array using the CMB concept. (a) Four CMB modules using COTS. (b) Indoor anechoic chamber measurements using a horn transmit antenna.

The resulting spectra of the mixed and combined signals for broadside and $\theta = 90°$ reception are given in Fig. 11. Notably, the spectra for each AoA are normalized at different power levels to highlight the achieved combining gain. Indeed, it is verified that CMB yields a maximum 3dB gain, implying coherent signal combining.

Also, we tested our CMB module in sub-array settings, as shown in Fig. 12. In this setup, two sub-arrays each two

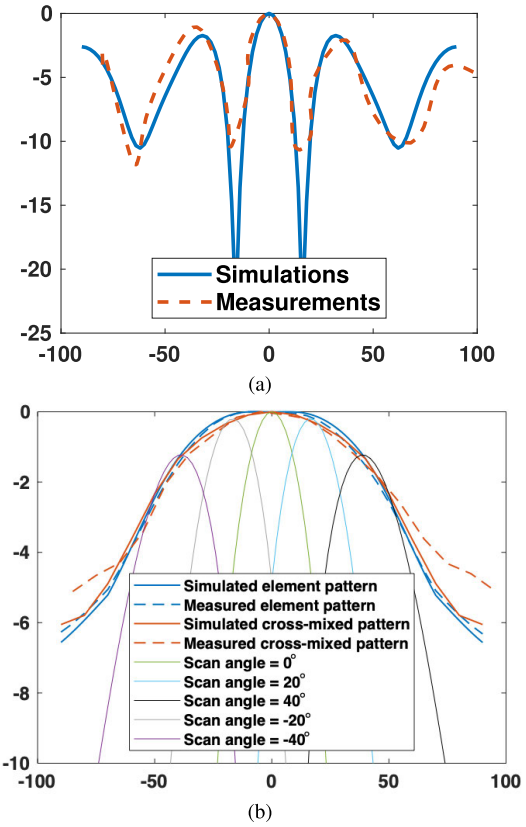

FIGURE 16. Simulated and measured cross-mixed patterns of a 4 × 2 monopole array (a) in a sub-array setting and (b) with 8-element CMB module.

elements each were considered. Again, the RF and the LO frequencies were 2.31 GHz and 1.89 GHz, respectively. This setup was tested for $\theta = 40°$. Fig. 13 shows the measured waveforms at the output of each sub-array after combining. It is clear that CMB retains the phase/time delays, $\Delta T_0 = 0.03332ns$ as captured by the oscilloscope.

This above implies a phase delay of $\Delta\phi_0 = 2\pi(f_{RF} + f_{LO})\Delta T_0 = 50°$ between the sub-arrays. This is equivalent to an angle of arrival of $\theta = 38.8°$. Accordingly, cross-mixing is capable of retaining the phase delay information between the sub-arrays.

B. TWO-DIMENSIONAL CROSS-MIXING

A 4×2 monopole antenna array was also fabricated for testing the CMB in a two-dimensional array setting (see Fig. 14a). The elements are subdivided into four separate sub-arrays, as shown in Figs. 14b and 15a. Each sub-array cross-mixes two elements together. The distance between adjacent elements is set to $d_x = \lambda_{RF}/2$ and $d_y = \lambda_{RF}/3$. Similarly, $f_{RF} = 2.31\ GHz$ and $f_{LO} = 1.89\ GHz$.

The monopole array was placed on a rotary positioner (see Fig. 15b). The latter allowed for measuring the cross-mixed pattern along the azimuth plane, as shown in Figs. 14 and 15.

The simulated and measured sub-array patterns are shown in Fig. 16a. We note that for both simulations and measurements, different AoAs were considered ranging

from −90° to 90°. Fig. 16a shows that the simulated and measured patterns are in good agreement. The slight fluctuations in the measurement are mainly due to fabrication tolerances and misalignment with the rotary positioner axis.

Finally, the 4 × 2 monopole antenna array was tested with a single 8-element CMB module, as shown in Fig. 14c. Here also, the measured pattern agrees closely with the simulation, as shown in Fig. 16b. Notably, the simulated cross-mixed pattern can be traced out by the beam-scanning patterns at the different AoAs. Importantly, Fig. 16b shows that cross-mixing self-adapts the element phases to the receiving AoA.

VII. CONCLUSION

We presented a novel hybrid beamforming configuration based on cross-mixing oppositely placed antenna elements to achieve coherent signal combining. This concept of phase delay cancellation is frequency independent and is highly flexible as compared to conventional beamformers. Prototypes were fabricated and tested in linear and planar array configurations. Importantly, CMB is compatible with hybrid beamformers and provides front-ends with enhanced degree of flexibility.

REFERENCES

[1] T. S. Rappaport, Y. Xing, G. R. MacCartney, A. F. Molisch, E. Mellios, and J. Zhang, "Overview of millimeter wave communications for fifth-generation (5G) wireless networks—With a focus on propagation models," *IEEE Trans. Antennas Propag.*, vol. 65, no. 12, pp. 6213–6230, Aug. 2017.

[2] V. Venkateswaran and A.-J. van der Veen, "Analog beamforming in MIMO communications with phase shift networks and online channel estimation," *IEEE Trans. Signal Process.*, vol. 58, no. 8, pp. 4131–4143, Aug. 2010.

[3] B. Widrow, P. E. Mantey, L. J. Griffiths, and B. B. Goode, "Adaptive antenna systems," *Proc. IEEE*, vol. 55, no. 12, pp. 2143–2159, Dec. 1967.

[4] S. Denno and T. Ohira, "Modified constant modulus algorithm for digital signal processing adaptive antennas with microwave analog beamforming," *IEEE Trans. Antennas Propag.*, vol. 50, no. 6, pp. 850–857, Jun. 2002.

[5] A. Hajimiri, H. Hashemi, A. Natarajan, X. Guan, and A. Komijani, "Integrated phased array systems in silicon," *Proc. IEEE*, vol. 93, no. 9, pp. 1637–1655, Sep. 2005.

[6] H. Hashemi, X. Guan, A. Komijani, and A. Hajimiri, "A 24-GHz SiGe phased-array receiver-LO phase-shifting approach," *IEEE Trans. Microw. Theory Techn.*, vol. 53, no. 2, pp. 614–626, Feb. 2005.

[7] A. Wiesel, Y. C. Eldar, and S. Shamai, "Zero-forcing precoding and generalized inverses," *IEEE Trans. Signal Process.*, vol. 56, no. 9, pp. 4409–4418, Sep. 2008.

[8] A. Gershman, N. Sidiropoulos, S. Shahbazpanahi, M. Bengtsson, and B. Ottersten, "Convex optimization-based beamforming," *IEEE Signal Process. Mag.*, vol. 27, no. 3, pp. 62–75, May 2010.

[9] J. Zhang, W. Wu, and D.-G. Fang, "Single RF channel digital beamforming multibeam antenna array based on time sequence phase weighting," *IEEE Antennas Wireless Propag. Lett.*, vol. 10, pp. 514–516, 2011.

[10] R. Miura, T. Tanaka, I. Chiba, A. Horie, and Y. Karasawa, "Beamforming experiment with a DBF multibeam antenna in a mobile satellite environment," *IEEE Trans. Antennas Propag.*, vol. 45, no. 4, pp. 707–714, Apr. 1997.

[11] E. Ali, M. Ismail, R. Nordin, and N. F. Abdulah, "Beamforming techniques for massive MIMO systems in 5G: Overview, classification, and trends for future research," *Frontiers Inf. Technol. Electron. Eng.*, vol. 18, no. 6, pp. 753–772, Jun. 2017.

[12] G. Kwon, Y. Shim, H. Park, and H. M. Kwon, "Design of millimeter wave hybrid beamforming systems," in *Proc. IEEE 80th Veh. Technol. Conf. (VTC-Fall)*, Vancouver, BC, Canada, Sep. 2014, pp. 1–5.

[13] T. E. Bogale, L. B. Le, A. Haghighat, and L. Vandendorpe, "On the number of RF chains and phase shifters, and scheduling design with hybrid analog–digital beamforming," *IEEE Trans. Wireless Commun.*, vol. 15, no. 5, pp. 3311–3326, May 2016.

[14] J. Nsenga, A. Bourdoux, and F. Horlin, "Mixed analog/digital beamforming for 60 GHz MIMO frequency selective channels," in *Proc. IEEE Int. Conf. Commun.*, Cape Town, South Africa, May 2010, pp. 1–6.

[15] O. E. Ayach, S. Rajagopal, S. Abu-Surra, Z. Pi, and R. W. Heath, Jr., "Spatially sparse precoding in millimeter wave MIMO systems," *IEEE Trans. Wireless Commun.*, vol. 13, no. 3, pp. 1499–1513, Mar. 2014.

[16] J. Kornprobst, T. J. Mittermaier, and T. F. Eibert, "A millimeter-wave self-mixing array with large gain and wide angular receiving range," *IEEE Trans. Antennas Propag.*, vol. 66, no. 2, pp. 702–711, Feb. 2018.

[17] J. L. Volakis, R. Hokayem, S. B. Venkatakrishnan, and E. A. Alwan, "Low power and reduced hardware UWB beamformers for future 5G communications," *IEICE Trans. Commun.*, vol. E102.B, no. 2, pp. 166–173, Feb. 2019.

[18] Y. Shoji, M. Nagatsuka, K. Hamaguchi, and H. Ogawa, "60 GHz band 64 QAM/OFDM terrestrial digital broadcasting signal transmission by using millimeter-wave self-heterodyne system," *IEEE Trans. Broadcast.*, vol. 47, no. 3, pp. 218–227, Sep. 2001.

[19] Y. Shoji, K. Hamaguchi, and H. Ogawa, "Millimeter-wave remote self-heterodyne system for extremely stable and low-cost broad-band signal transmission," *IEEE Trans. Microw. Theory Techn.*, vol. 50, no. 6, pp. 1458–1468, Jun. 2002.

[20] R. A. Pacheco and D. Hatzinakos, "BER analysis of self-heterodyne OFDM transmission scheme," in *Proc. Can. Conf. Electr. Comput. Eng.*, vol. 4, 2004, pp. 1953–1956.

[21] S. Maier, X. Yu, H. Schlesinger, G. Luz, P. Juschke, U. Seyfried, and A. Pascht, "Phase noise cancellation performance in self-heterodyning transceivers for wireless backhaul applications," in *Proc. IEEE Radio Wireless Symp. (RWS)*, Jan. 2015, pp. 196–199.

[22] J.-Y. Kim and W.-Y. Choi, "30 GHz CMOS self-oscillating mixer for self-heterodyne receiver application," *IEEE Microw. Wireless Compon. Lett.*, vol. 20, no. 6, pp. 334–336, Jun. 2010.

[23] P. Burasa, N. G. Constantin, and K. Wu, "Low-power injection-locked zero-IF self-oscillating mixer for high Gbit/s data-rate battery-free active μRFID tag at millimeter-wave frequencies in 65-nm CMOS," *IEEE Trans. Microw. Theory Techn.*, vol. 64, no. 4, pp. 1055–1065, Apr. 2016.

[24] H. Gao, M. K. Matters-Kammerer, and P. G. M. Baltus, "A 60 GHz low power self-mixing receiver in 65-nm CMOS for a radio-triggered battery-less monolithic wireless sensor," *IEEE J. Emerg. Sel. Topics Circuits Syst.*, vol. 8, no. 2, pp. 240–250, Jun. 2018.

[25] W.-Z. Chen, T.-Y. Lu, W.-W. Ou, S.-T. Chou, and S.-Y. Yang, "A 2.4 GHz reference-less receiver for 1 mbps QPSK demodulation," *IEEE Trans. Circuits Syst. I, Reg. Papers*, vol. 59, no. 3, pp. 505–514, Mar. 2012.

[26] M. Novak, S. B. Venkatakrishnan, and J. Volakis, "Frequency-independent receiver and beamforming technique," U.S. Patent 10 439 851, Oct. 8, 2019.

[27] R. Hokayem, E. Alwan, and J. Volakis, "Cross-mixing beamformer," U.S. Patent 10 680 694, Jun. 9, 2020.

[28] T. J. Brockett and Y. Rahmat-Samii, "Subarray design diagnostics for the suppression of undesirable grating lobes," *IEEE Trans. Antennas Propag.*, vol. 60, no. 3, pp. 1373–1380, Mar. 2012.

RIMON HOKAYEM (Graduate Student Member, IEEE) received the master's degree in telecommunications engineering from the Lebanese University - Faculty of Engineering II, Roumieh, Lebanon, in 2014. He is currently pursuing the Ph.D. degree in electrical engineering with the Department of Electrical and Computer Engineering, Florida International University, Miami, FL, USA. He completed his master's project during his internship at Centre de Sciences Nucléaires et de Sciences de la Matière (CSNSM/IN2P3/CNRS), Ile-de-France, France. His thesis focused on field-programmable gate array (FPGA) programming for data acquisition and processing of gamma-rays. His research interests include radio frequency systems with an emphasis on beamforming and reduction in hardware and power consumption.

SANDHIYA REDDY GOVINDARAJULU (Graduate Student Member, IEEE) received the B.E. degree in electronics and communication engineering and the M.E. degree in communication systems from Anna University, Chennai, India, in 2013 and 2015, respectively. She is currently pursuing the Ph.D. degree with Florida International University, Miami, FL, USA. She was an Intern Researcher with the Society for Applied Microwave Electronics Engineering and Research, India, during her master's degree studies. She was a Program Analyst with Cognizant Technology Solutions, Chennai. Her research interests include millimeter-wave antennas for 5G communication systems, beamforming, and RF front end. She received the Best Student Paper Award for her research work at iWAT 2019.

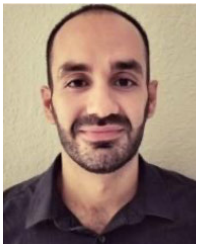

ELIAS A. ALWAN (Member, IEEE) was born in Aitou, Lebanon, in 1984. He received the B.E. degree *(summa cum laude)* in computer and communication engineering from Notre Dame University–Louaize, Zouk Mosbeh, Lebanon, in 2007, the M.E. degree in electrical engineering from the American University of Beirut, Beirut, Lebanon, in 2009, and the Ph.D. degree in electrical and computer engineering from The Ohio State University (OSU), Columbus, OH, USA, in 2014. From 2015 to 2017, he was a Senior Research Associate with the ElectroScience Laboratory, OSU. He is currently an Assistant Professor with the Electrical and Computer Engineering Department, Florida International University. His research interests include antennas and radio frequency systems with particular focus on ultra-wideband (UWB) communication systems, including UWB arrays, reduced hardware and power efficient communication back-ends, and millimeter-wave technologies for 5G applications. Since 2010, he has been a Phi Kappa Phi member.

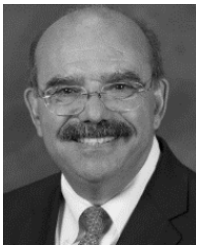

JOHN L. VOLAKIS (Fellow, IEEE) was born in Chios, Greece, in May 1956. He received the B.E. degree *(summa cum laude)* from Youngstown State University, Youngstown, OH, USA, in 1978, and the M.Sc. and Ph.D. degrees from The Ohio State University, Columbus, OH, in 1979 and 1982, respectively. From 1982 to 1984, he was with Rockwell International (currently Boeing), El Segundo, CA, USA. He was appointed as an Assistant Professor with the University of Michigan, Ann Arbor, MI, USA, in 1984, where he became a Full Professor, in 1994. From 1998 to 2000, he was the Director of the Radiation Laboratory, El Segundo. From January 2003 to August 2017, he was the Roy and Lois Chope Chair Professor of Engineering with The Ohio State University, where he was the Director of the Electroscience Laboratory, from 2003 to 2016. Since August 2017, he has been the Dean of the College of Engineering and Computing and a Professor of electrical and computer engineering with Florida International University (FIU). He has graduated/mentored nearly 95 doctoral students/postdoctoral with 41 of them receiving best paper awards at conferences. His publications include eight books, 425 journal articles, nearly 850 conference papers, 31 book chapters, and 21 patents/patent disclosures. His coauthored books are *Approximate Boundary Conditions in Electromagnetics* (1995), *Finite Element Methods for Electromagnetics* (1998), *Antenna Engineering Handbook* (Fourth Edition, 2007 and Fifth Edition, 2009), *Small Antennas* (2010), and *Integral Equation Methods for Electromagnetics* (2011). His current research interests include antennas, wireless communications and propagation, computational methods, electromagnetic compatibility and interference, design optimization, radio frequency (RF) materials, multiphysics engineering, millimeter waves, terahertz, and medical sensing. He is a Fellow of the Applied Computational Electromagnetics Society (ACES). He was a recipient of The University of Michigan College of Engineering Research Excellence Award, in 1993, Scott Award from The Ohio State University College of Engineering for Outstanding Academic Achievement, in 2011, the IEEE AP Society C-T. Tai Teaching Excellence Award, in 2011, the IEEE Henning Mentoring Award, in 2013, the IEEE Antennas & Propagation Distinguished Achievement Award, in 2014, The Ohio State University Distinguished Scholar Award, in 2016, and The Ohio State University ElectroScience George Sinclair Award, in 2017. His service to Professional Societies includes the 2004 President of the IEEE Antennas and Propagation Society, in 2004, the Chair of the USNC/URSI Commission By, from 2015 to 2017, twice the General Chair of the IEEE Antennas and Propagation Symposium, the IEEE APS Distinguished Lecturer, the IEEE APS Fellows Committee Chair, and the IEEE-wide Fellows Committee Member. He is an associate editor of several journals. He was listed by ISI among the top 250 most referenced authors, in 2004.